ACS OMEGA

http://pubs.acs.org/journal/acsodf

Article

Fibrous TiO_2 Alternatives for Semiconductor-Based Catalysts for Photocatalytic Water Remediation Involving Organic Contaminants

Daliane R. C. da Silva, Sivuyisiwe Mapukata, Sara Currie, Alexandros A. Kitos, Anabel E. Lanterna, Tebello Nyokong,* and Juan C. Scaiano*

Cite This: *ACS Omega* 2023, 8, 21585−21593

Read Online

ACCESS | Metrics & More | Article Recommendations | Supporting Information

ABSTRACT: Water decontamination remains a challenge in several developed and developing countries. Affordable and efficient approaches are needed urgently. In this scenario, heterogeneous photocatalysts appear as one of the most promising alternatives. This justifies the extensive attention that semiconductors, such as TiO_2, have gained over the last decades. Several studies have evaluated their efficiency for environmental applications; however, most of these tests rely on the use of powder materials that have minimal to no applicability for large-scale applications. In this work, we investigated three fibrous TiO_2 photocatalysts, TiO_2 nanofibers (TNF), TiO_2 on glass wool (TGW), and TiO_2 in glass fiber filters (TGF). All materials have macroscopic structures that can be easily separated from solutions or that can work as fixed beds under flow conditions. We evaluated and compared their ability to bleach a surrogate dye molecule, crocin, under batch and flow conditions. Using black light (UVA/visible), our catalysts were able to bleach a minimum of 80% of the dye in batch experiments. Under continuous flow experiments, all catalysts could decrease dye absorption under shorter irradiation times: TGF, TNF, and TGW could, respectively, bleach 15, 18, and 43% of the dye with irradiation times as short as 35 s. Catalyst comparison was based on the selection of physical and chemical criteria relevant for application on water remediation. Their relative performance was ranked and applied in a radar plot. The features evaluated here had two distinct groups, chemical performance, which related to the dye degradation, and mechanical properties, which described their applicability in different systems. This comparative analysis gives insights into the selection of the right flow-compatible photocatalyst for water remediation.

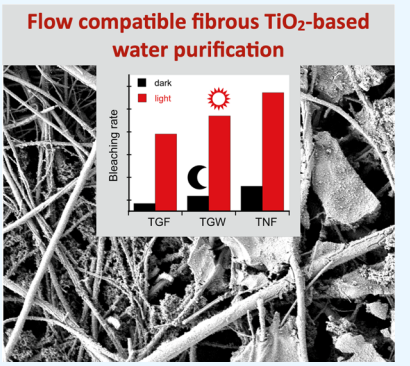

INTRODUCTION

Universal access to safe water is still a major challenge for nations around the globe. According to the United Nations, the lack of sufficient water treatment plants and sanitation is responsible for letting more than 1.5 billion people consume unsafe water every year.[1] Human activities are one of the main sources of contamination, introducing a growing number of compounds into the water bodies. Such contaminants range from pathogens, heavy metal ions, and organic pollutants.[1−3] Among the latter are pharmaceuticals, endocrine disrupters, personal care products, dyes, phenols, and benzene compounds.[1,4−6] Addressing this challenge calls for affordable and efficient alternatives while being safe for humans and having minimal environmental impact.

Among the most promising alternatives for water remediation, the use of heterogeneous catalysts is one of the most developed alternatives due to their stability, low cost, and nontoxicity. Since the discovery of photocatalytic water splitting using TiO_2, in 1972, by Honda and Fujishima,[7,8] this semiconductor had gained great attention for photocatalytic uses. It is widely used for energy purposes and environmental applications.[9−11] Its large band gap (3.19 eV) gives it enough energy to perform catalytic reactions that require large energy inputs, such as water oxidation and radical formation. In particular, hydroxyl radicals and other radicals originating from them are of great interest due to their high antimicrobial nature,[12] which also finds utilization in degrading organic materials. These two applications combined can make TiO_2 a promising catalyst for water remediation.[13−15]

Most of the research has been performed with powder TiO_2, frequently commercial P25 grade, which is mostly anatase phase with particles of around 25 nm in size. This is generally suitable for small-scale batch applications, and many interesting "proof-of-concept" reports are available.[16−22] For environmental applications, particularly if they involve water treatment, batch strategies with powder catalysts are unlikely to find practical applications. For this, flow methods are essential for suitable scale-up to be viable. Further, if illumination is required, batch systems present additional challenges because

Received: February 6, 2023
Accepted: May 25, 2023
Published: June 8, 2023

of limited light penetration and the need for surface exposure to incident light. In our recent research, we have found that fibrous materials, including TiO_2-rich components have excellent properties for flow catalysis, as they present a fixed bed catalyst, that allows liquids to flow without loss of catalytic materials.[23] In a typical test, the fibrous material is not exposed to mechanical challenges, so they simply need to be robust enough to maintain their integrity in the presence of liquid flow, a frequently reducing environment and simultaneous illumination.[23]

Flow-suitable catalysts can be achieved by the preparation of fibrous TiO_2, such as nanofibers and microfibers,[24−26] or by using a support material to deposit the TiO_2 photocatalyst. The latter is a supported catalyst. The *in situ* synthesis, deposition, impregnation, and precipitation of catalytic materials on inert surfaces introduce compatibility with flow systems and thus easy separation from solutions. Some of the supports developed include glass wool, glass beads, glass filters, and cellulose filters.[16,22,23,27−29]

In our group, we are investigating the use of glass supports for titanium dioxide, due to their inert, nontoxic, and inexpensive characteristics. In this contribution, we tested three TiO_2-rich materials. The first one consists of TiO_2 fibers (about 1 μm diameter) produced by electrospinning (TiO_2NF). The other two materials are preceded by *in situ* depositing TiO_2 on glass fibers. In one of them, the substrate is glass wool pretreated with APTES with fibers of about 10 μm in diameter (TiO_2@GW), and in the other, TiO_2 was deposited on glass filters, a fibrous cardboard-like material consisting of glass fibers of about 100 nm in diameter. Our tests include bleaching of an organic dye, crocin, which is the pigment present in saffron. For illumination, we use 30 cm long black light (UVA/Visible ∼400 nm), a safe source, that emits at the edge of the absorption profile of TiO_2. Our work involves batch studies and a bench-scale flow system to evaluate and compare these materials aiming at future applications in large-scale flow systems. Here, we compared and discussed the performance of those materials using parameters such as flow compatibility, availability, convenience (including synthesis), photochemical activity, mechanical properties, and reusability.

MATERIALS AND METHODS

Materials. Unless otherwise specified, all chemicals and glass wool fibers were purchased from Sigma-Aldrich and used without further purification. Glass fiber filters were purchased from Pall Corporation and APTES (3-aminopropyl triethoxysilane) from Tokyo Chemical Industry Co., Ltd. (TCI).

Catalyst Preparation. *TiO_2 Nanofibers (TNF).* A 10% PVP (polyvinylpyrrolidone) solution was prepared in 20 mL of ethanol (EtOH) with vigorous stirring for 2 h. A mixture of 5 mL (60 mM) of TiP (titanium isopropoxide) and 5 mL of acetic acid was made by stirring them until a transparent solution was obtained, which was then added to the PVP/EtOH solution, followed by vigorous stirring for 8 h. This polymeric solution was loaded into a 20 mL plastic syringe for electrospinning. Fibers were spun applying a positive voltage of 18 kV at the needle tip with respect to the collector metal (aluminum tray) with a tip to collector distance (TCD) of 12 cm. A syringe pump was used to flow the solution at a flow rate of 1 mL/h. After the entire solution was spun, the collected material was removed from the aluminum tray and calcined to obtain anatase TiO_2. The calcination was done under air, at 500 °C for 2 h.

TiO_2@Glass Wool (TGW). A 10% PVP solution was prepared in 20 mL of EtOH with vigorous stirring for 2 h. A mixture of 5 mL (60 mM) of titanium isopropoxide and 5 mL of acetic acid was made by stirring them until a transparent solution was obtained, which was then added to the PVP/EtOH solution, followed by vigorous stirring for 2 h. The TiO_2 precursor solution was added to a 30 cm glass tube, with 1.5 g of HCl (6 M) and APTES-treated glass wool as previously described.[23] The solution was stirred using a rotator overnight at room temperature; the slow rotation ensured adequate mixing without mechanical stress for the fibers. After this period, the glass wool was removed and carefully washed 3× with EtOH and 3× with distilled water and left to dry in an oven at 80 °C overnight. The dry TGW was then calcined under air using a tube furnace heated at 500 °C for 2 h, followed by 5 min at 600 °C. The material was left to cool down at room temperature, washed 5× or until a clear solution is obtained with distilled water, and dried at 80 °C.

TiO_2@glass Filter (TGF). A TGF catalyst was synthesized directly onto the glass fiber filter. Glass fibers (with long fibers about 300 nm in diameter) were cut by hand into strips (0.60 cm in width and ranging from 5.50 to 25.0 cm in length) using ceramic scissors to avoid contamination. These were weighed and placed in an aluminum foil tray. Once in the tray, 3−5 mL of TiP was added on both sides of the filter strips to ensure saturation. Following this, the aluminum tray was filled with deionized water. The saturated strips were left submerged in water for 15 min, on each side. The loaded filter strips were then removed from the aluminum tray and placed between two sheets of aluminum foil. Using a clothing iron, the sandwiched filter strips were ironed at medium heat (140−160 °C) until dry. To obtain anatase TiO_2, the dried glass filter strips of TiO_2 supported on the glass fiber filter paper were placed inside a tube furnace and heated at 500 °C for 2 h, followed by 5 min at 600 °C. The material was left to cool down at room temperature, washed 5× or until a clear solution is obtained with distilled water, and dried at 80 °C.

Photocatalytic Activity. The photocatalytic performance of the three catalysts was evaluated using UVA/visible black light composed of nine LEDs with maximum emission at 400 nm (Viugreum). The irradiance of each LED was measured at a 3 cm distance using a spectroradiometer (Luzchem, SPR-4002, Ottawa, Canada). The energy distribution for a single LED is described in Table 1.

Table 1. Energy Distribution of a Single LED Measured with a Spectroradiometer

region	power W/m^2
UVB	traces
UVA	12.9
visible	5.1
total	18.0

Characterization. SEM images were acquired using a JSM-7500F field emission scanning electron microscope from JEOL Ltd. Elemental identification mapping was done using a Zeiss Gemini SEM 500 equipped with an energy-dispersive X-ray spectrometer (EDS) system (QUANTAX, Bruker). Diffuse reflectance (DR) measurements were carried out in VARIAN Cary 100 UV−vis spectrophotometer coupled with an

https://doi.org/10.1021/acsomega.3c00781
ACS Omega 2023, 8, 21585−21593

integrating sphere accessory, and absorption spectroscopy was performed in a Cary-60 UV-visible spectrophotometer. Fourier transform infrared (FTIR) spectra were obtained on a Nicolet IS5 FTIR spectrometer equipped with an iD7 attenuated total reflectance (ATR) accessory. For each sample, 64 scans were recorded with resolution of 4 cm^{-1}. Powder X-ray diffraction analysis was carried out at room temperature on a Rigaku Ultima IV powder diffractometer in Bregg Brentano geometry, using Cu Kα radiation (λ = 1.5418 Å). Two theta range of 20−90° was covered with 0.02° step width and 0.5°/min scan speed. The specific surface area was measured using the Brunauer−Emmett−Teller (BET) N_2 isotherms collected on a Micromeritics 3Flex adsorption analyzer at 77 K (liquid N_2 bath). Prior to measurements, all samples (0.030−0.050 g) were activated using a Micromeritics Smart VacPrep under a high vacuum at 100 °C for 24 h. We aimed to study the charge separation using a photoluminescence technique. But the glass wool utilized has luminescence that interferes with the emission from TiO_2 (Figure S13); thus, we decided not to use this technique to compare the photocatalysts used.

Degradation of an Organic Dye. The photocatalytic activity of the fibrous TiO_2 materials was evaluated by following the photodegradation of crocin ($C_{44}H_{64}O_{24}$, see Scheme S1); we note that "degradation" does not imply complete mineralization. The reaction vessel was maintained at ambient temperature. In a typical experiment, aqueous solutions of crocin (5 mL, 8.1 μM) were mixed with the fibrous TiO_2 catalysts in a glass vial. Since each material has different TiO_2 loading, we weighed the materials to obtain a final concentration of 10 mg/mL of TiO_2 in the solution. The solutions were stirred constantly, using a microplate shaker. Before irradiation, the suspension was kept in the dark to establish adsorption/desorption equilibrium. At 30 min intervals, 1 mL of the suspension was collected, and dye absorbance was measured. The change in absorbance at 440 nm was plotted against time.

Degradation under an inert atmosphere was run similarly to the batch experiments. Samples were purged with N_2 for 20 min prior to illumination. During the 3 h of the experiment, samples had N_2 balloons attached to guarantee the inert atmosphere.

We note that methylene blue is a frequent choice for photodegradation work. However, we noted that methylene blue absorbs strongly on glass-based materials, thus masquerading as dark bleaching of the dye. This led to the choice of crocin as the dye for degradation studies.

Reuse of TiO_2 Catalysts. To study the reusability of the catalysts, all of the experimental parameters were kept constant, and the experiments were repeated for 5 sets using the same catalyst and fresh dye solutions. After each photodegradation assay, the catalyst was rinsed with distilled water to remove any organic contaminant. The catalysts were dried at 100 °C overnight before each use.

Continuous Flow Degradation. Flow experiments were performed in a bench-scale system. Catalysts were placed inside a 15.9 cm long tube (I.D.: 3 mm) connected through a PVC tubing (I.D.: 4 mm). Catalyst amounts were set to obtain 8 mg of TiO_2 inside the tube. A total volume of 20 mL of crocin solution was fed into the system using a syringe pump (NE-300 Just Infusion Syringe Pump) at 10, 30, 50, or 100 mL/h. The solution flowed in the dark until a steady state was achieved. For irradiation experiments, the tube was placed between two UVA/Visible black light, and three LEDs from each lamp were used as light sources, while the other six LEDs were covered with aluminum foil. Residence time (the time in which the solution spends in contact with the catalyst and is exposed to light) was determined by dividing the volume of the flow tube by the flow rate. Note that due to the different volumes filled by catalyst itself, the total liquid capacity inside of the tube is different for each material. The total exposure (from three LEDs) is thus three times that indicated in Table 1. The outlet samples were examined every minute using a Cary-60 spectrometer equipped with a flow cuvette that allows in-line monitoring. The absorbance at λ = 440 nm was recorded and compared with the initial absorbance of the crocin solution.

High-performance Liquid Chromatography (HPLC) Analysis. To evaluate the resulting solution, from the single-pass flow experiment, we irradiated an aqueous solution of crocin 1 mM in the presence of TGW until 90% of bleaching was observed. The treated solution was then evaluated using high-performance chromatography. HPLC was performed on an Agilent 1260 infinity II series HPLC instrument, using a ZORBAX SB-C18 column (2.1 × 50 mm−1.8 μm particle size). Acetonitrile and water were used as mobile phase using the gradual change from 10:90 (acetonitrile:water) to 80:20 at a of flow rate of 1 mL/h.

RESULTS AND DISCUSSION

Characterization. The use of photocatalysts in water remediation is generally limited by their powder morphology, which makes it hard to separate them from solution and is not suitable for flow reactors. Knowing the importance and effectiveness of TiO_2, we designed three new fibrous TiO_2 materials that are compatible with flow systems. For all materials, TiO_2 was fabricated *in situ* using titanium isopropoxide as a precursor, followed by calcination. Titanium dioxide nanofibers (TNF) were made up of only TiO_2. The two catalysts on glass supports, TiO_2 on glass wool (TGW) and on glass filter (TGF) had TiO_2 loading determined gravimetrically. TGW has 48% and TGF has 62% of the semiconductor. Photographs of the materials can be found in Figure S1; all fibrous materials have large macroscopic structures and can be easily removed from the reactions using tweezers or stay in flow tubes without moving with the solutions. TiO_2 nanofibers were made with support polymer (PVP), which was used to give the viscosity to the precursor solution, allowing it to be electrospun and as support for the semiconductor precursor. Before calcination, fibers had an average diameter of 1.5 μm (±0.3 μm) (Figure S3A), which decreased to 0.98 μm (±0.4 μm) after annealing. Macroscopically, the fibers had a flake-like shape and were very light.

Using the same polymer support (PVP) and precursor solution for the nanofibers, we loaded TiO_2 to the APTES-treated glass wool (9.4 ± 1.8 μm), giving the catalyst a fibrous support. APTES was bonded to the glass through the silicon moieties, leaving free amino groups on the glass surface, which undergo hydrogen bonding with the available hydroxyl groups on TiO_2.[30] Calcination at 500 °C allows the formation of crystalline TiO_2 without damaging the glass. Tests with different annealing temperatures (data not shown) demonstrated that at temperatures closer to the GW melting point (680 °C), the semiconductor had better adherence to the support. Thus, we selected a short time at 600 °C to avoid the conversion of anatase into the rutile form of TiO_2. After synthesis, TiO_2 can be seen covering and connecting the glass

https://doi.org/10.1021/acsomega.3c00781
ACS Omega 2023, 8, 21585−21593

wool fibers (Figure 1B). Close-up photos comparing the original support and the final material highlight the presence of

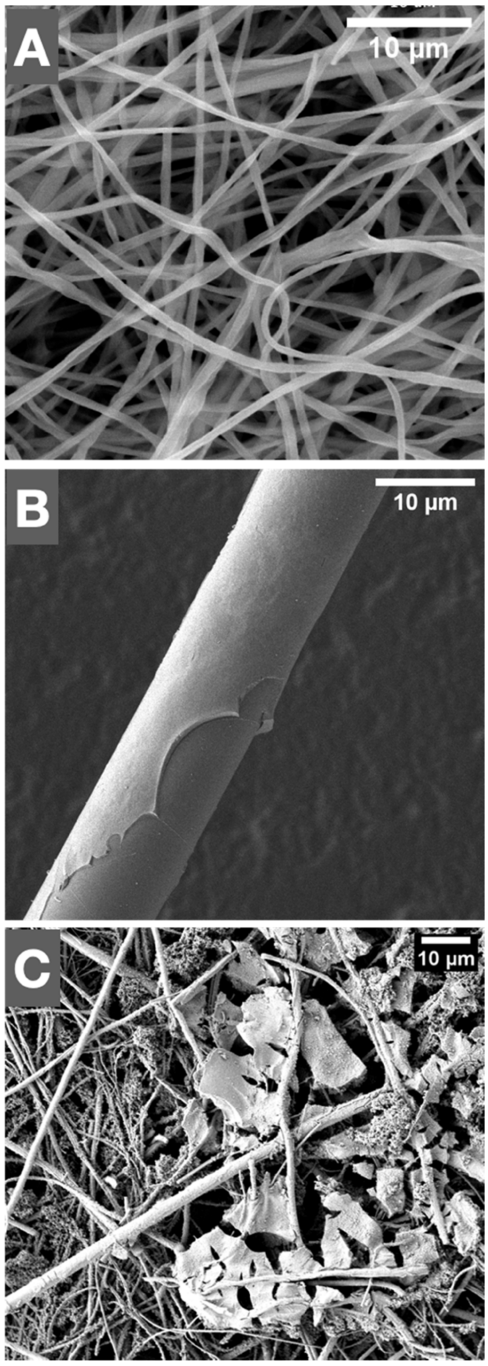

Figure 1. Representative SEM images of fibrous TiO_2: (A) TiO_2 nanofibers (TNF), (B) TiO_2 deposited on a glass wool fiber (TGW), and (C) TiO_2 deposited on glass filter fibers (TGF). All of the SEM images were taken after material calcination at 500 °C.

a TiO_2 net in the fabricated material (Figure S2). Using SEM, we can also observe that TiO_2 formed a film-like coverage on the fibers (Figure 1B). At breakage spots, the fiber and its coating are readily distinguishable. The location of the semiconductor on the glass support is further confirmed using EDS mapping (Figure S4).

The third material, TiO_2@glass filter (TGF), used commercially available glass fiber filters as a support. Originally the glass fibers had a diameter of 0.36 μm with a polydisperse size distribution. After TiO_2 addition, we can see that the photocatalyst was deposited between the glass fibers on the support (Figures 1C and S5). Moreover, even after the TiO_2 treatment, the final material maintained the macroscopic features of the original glass filter (Figure S1). Different from the previous TGW, no APTES treatment was required in this case since the intricate glass fiber arrangement was able to retain the semiconductor.

FITR spectra of the fiber photocatalysts can be found in the Supporting Information (Figure S7). For the materials containing glass (TGW and TGF), we can see the characteristic bands for silicate glass, with the prominent vibration band at ~1000 cm^{-1} for the asymmetric stretch of Si−O, the weak band at ~800 cm^{-1} assigned to the Si−O bending, and the band at ~480 cm^{-1} corresponding to the rocking bend of Si−O−Si. Note that the vibration at ~1000 cm^{-1} is shifted between the two glass materials (GW and GF). This band is the most sensitive to changes in the structure since it is affected by the Si−O−Si bonding angle. In all samples containing TiO_2 (TNF, TGF, and TGW), we see the band corresponding to Ti−O stretching located at ~438 cm^{-1}. In glass containing samples, this band is overlapped with the Si−O−Si rocking vibration from the support.

X-ray diffractograms reveal that all materials are composed of the anatase crystalline phase, which is the most photocatalytically active.[31−34] The position of the peaks at 2θ = 25.4, 37.9, 48.1, 55.05, 55.2, and 62.9° correspond to the respective planes (101), (004), (200), (105), (211), and (204) of tetragonal anatase TiO_2 (JCPDS: 01-073-1754), Figure 2A. Using the Scherrer equation, we calculated the crystalline sizes of the photocatalysts finding 13.2, 10.3, and 9.5 nm for TNF, TGW, and TGF, respectively. Interestingly, TGW and TGF, which were treated at 600 °C for 5 min did not show any peak corresponding to the rutile phase, which is the most thermally stable form. Lastly, optical properties were measured with diffuse reflectance. As expected for anatase TiO_2, all three materials have strong absorbance in the UVA range (Figure 2B) with band gaps between 3.12 and 3.22 eV (Figure S8), in agreement with typical values for anatase TiO_2. The emission of the light source chosen for the experiments can also be seen in Figure 2b (dashed line). The maximum at 400 nm matches with the absorption tail of the nanostructures, utilizing the photocatalyst ability of this semiconductor while keeping emission at a safer wavelength for users.

Part of the catalyst efficiency is defined by its surface area. To compare these catalysts, we analyzed the N_2 isotherms using the Brunauer−Emmett−Teller (BET) method to obtain their specific surface area (SSA). All materials revealed typical type IV isotherms (according to IUPAC classification) with a hysteresis loop (capillary condensation).[35] Table 2 summarizes the results for all of the fibrous materials, before and after TiO_2 treatment (when applicable). The first observation is the difference between the SSA of both glass supports alone, glass filter and glass wool. The larger surface area of the glass fiber filters justifies the higher loading of TiO_2 when compared with TGW. Moreover, for the glass wool, the addition of APTES not only created better adherence to TiO_2 but also led to some increase in the surface area of the material.

TGF had the higher surface area out of the three TiO_2-rich materials with 25.02 m^2/g, followed by TGW and TNF with 17.4 and 15.8 m^2/g, respectively. Part of this difference is justified by the crystallite sizes of each material, where smaller

https://doi.org/10.1021/acsomega.3c00781
ACS Omega 2023, 8, 21585−21593

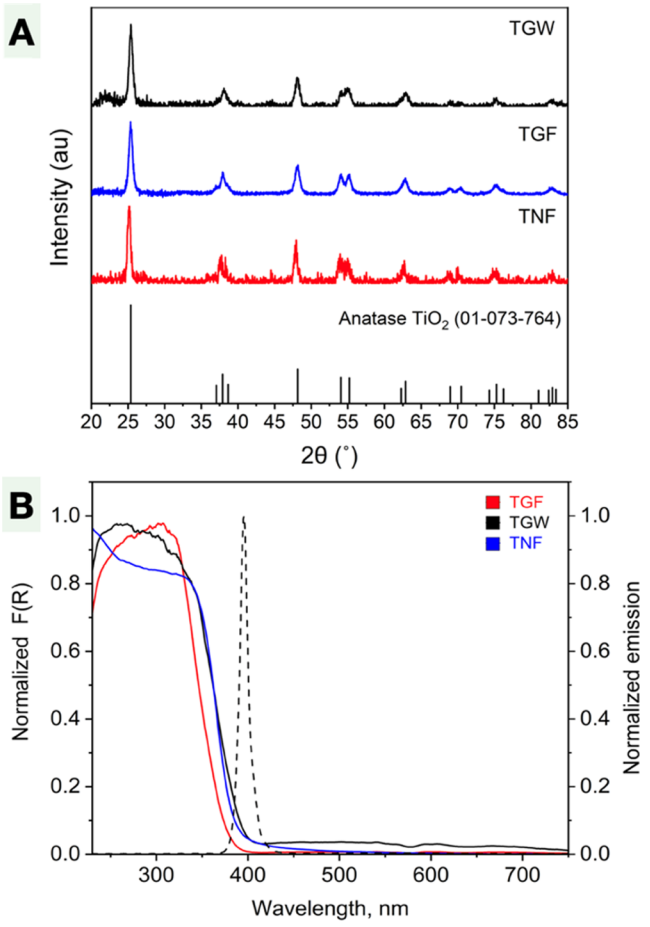

Figure 2. (A) X-ray powder diffraction (XRD) patterns of the produced fibrous materials: TiO_2 NF (red), TiO_2@GF (blue), and TiO_2@GW (black) and the PDF card 01-073-1764 pattern. (B) Normalized diffuse reflectance of the fibrous TiO_2 materials (solid line) and emission of the black light used in the experiments (dashed line). Tauc plots are shown in Figure S8.

Table 2. Specific Surface Area (m^2/g) of the Fibrous Catalysts and Their Support Materials (If Applicable)[a]

sample	SSA (m^2/g)
TNF	15.8 ± 0.2
GF	20.2 ± 0.4
TGF	25.0 ± 0.7
GW	6.8 ± 0.2
APTES-GW	12.4 ± 0.2
TGW	17.4 ± 0.3

[a]Obtained by BET analysis of the N_2 adsorption−desorption isotherms acquired at 77 K.

crystallite sizes lead to larger SSA.[36] Among the three materials, TGF had the smaller average crystallite sizes (9.5 nm). Another reason is the presence and type of glass support. We can see that GF alone had already a large surface area that was impregnated with the semiconductor. Interestingly, for both glass-supported catalysts, the addition of TiO_2 increased the total surface area of the material, which is due to the higher porosity of TiO_2, when compared to the glass supports.

Crocin Degradation. While all of the catalysts are flow-compatible, we developed a set of batch experiments in small batch systems to evaluate catalyst performance. We used crocin, a carotenoid extracted from Saffron, as a surrogate molecule. The high presence of delocalized electrons makes it strongly absorbent in the visible range with a maximum at 440 nm (Figure S14—dashed line). Under light irradiation (λ ~400 nm, 18 W/m^2 for each of the nine LEDs), crocin solution alone (8.1 μM in water) bleaches slowly, ~20% during 3 h of light exposure (Figure S9), probably mediated by singlet oxygen.[37,38]

The dye solution and catalysts were incubated in the dark for 3 h to allow adsorption equilibration. Change in absorbance in the dark can be seen in Figure 3A. The dark adsorption order followed the SSA order for all of the materials (Figure 4). Catalysts were impregnated with the yellow dye, in

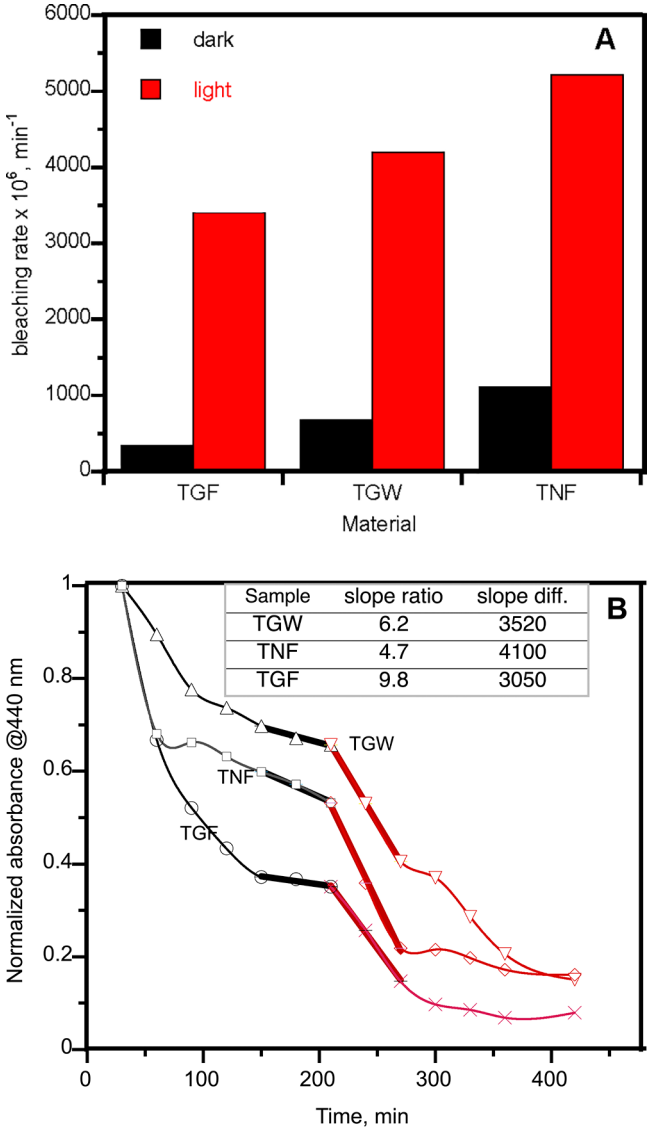

Figure 3. (A) Crocin bleaching rates, in the dark (black) and under irradiation using a black light (red), in the presence of the fibrous TiO_2-rich materials. Crocin remaining based on the absorbance at 440 nm over time. (B) Decay of crocin absorption as a function of time in the presence of the fibrous TiO_2-rich materials. Insert: slope ratio and the difference between dark and light treatment for the three fibrous catalysts. Slopes (rates) are based on the last three points (black heavy line) before turning on the 400 nm light and the three points immediately after the lights are turned on (red heavy line). All rates in units of 10^{-6} min^{-1}.

https://doi.org/10.1021/acsomega.3c00781
ACS Omega 2023, 8, 21585−21593

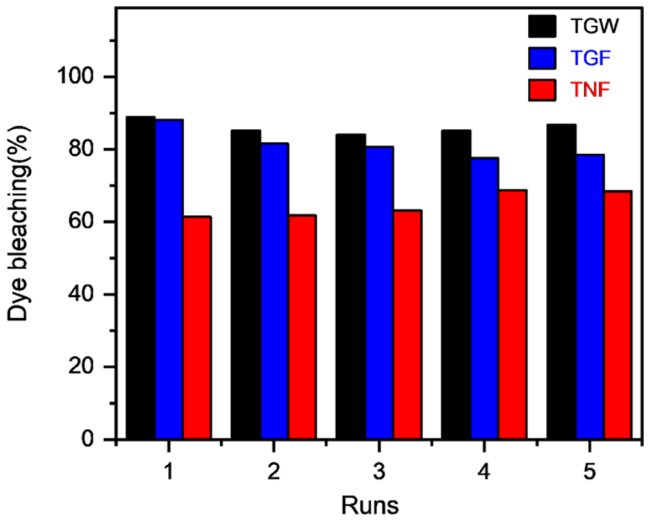

Figure 4. Reusability test results of the 5 cycles of crocin bleaching, followed at 440 nm. Experiments run in batch with an initial dye concentration of 8.1 μM and under UVA irradiation (18 W/m^2).

particular TGF that had the highest surface area (Figure S10), proving that the bleaching in the dark is due to adsorption on the photocatalyst.

As the light was turned on (at 200 min), the degradation rate increased (Figure 3B), and after 3 h of irradiation (18 W/m^2), the maximum absorbance dropped 84% in the presence of TNF, 85% for TGW, and 92% for TGF. It is noteworthy that the higher degradation rates are related to the materials showing absorption profiles that overlap better with the excitation wavelengths (*cft.* Figures 2B and S7). Mechanistically, irradiation on the photocatalyst generates electron−hole pairs, which can, respectively, reduce and oxidize other molecules such as water, O_2, and the dye itself. TiO_2-mediated organic dye degradation is a result of the redox reactions mediated by the photogenerated electrons/holes, adsorption on the catalyst, and, in the case of visible light irradiation, the excitation of the dye itself. The latter was previously studied elsewhere, which showed that excited electrons generated by the dye can be transferred to the photocatalyst assisting the degradation. However, this mechanism is less prevalent than the direct excitation on the photocatalyst.[39,40]

To better understand the mechanisms behind the dye bleaching, we first evaluated the $^{\bullet}$OH production among all catalysts. We used coumarin, which is a probe that is oxidized by hydroxyl radicals forming 7-hydroxycoumarin (7-HC), which has strong fluorescence at 454 nm (ex = 332 nm).[41] The emission spectrum from the production of 7-HC is in the Supporting Information (Figure S11). After 3 h of dark incubation, the fluorescence produced by all catalysts is approximately the same as time zero (T_0), showing that light is necessary to induce the formation of hydroxyl radicals from the catalyst. Samples that were irradiated had increasing fluorescence emission over time. The higher fluorescence from the samples treated with TGF, especially because their degradation rates were lower than the other materials was noticeable. TGF has a significantly higher SSA (Table 1), which increases the chances of the encounter between the target molecules adsorbed on the catalyst and the short-lived photogenerated holes and $^{\bullet}$OH. The latter tends to react with nearby molecules with virtually no selectivity. Further we evaluated crocin photodegradation under anaerobic conditions. In the absence of oxygen, there is a decrease of the overall photocatalytic activity (Figure S12). The 8.2, 22.3, and 33.9% decrease in photocatalytic activity for TNF, TGW, and TGF, respectively, emphasizes that most of the bleaching is not O_2-related, possibly by OH radicals and by the adsorption of the dye on the catalyst. In the absence of oxygen, the lower bleaching values can be assigned to the decrease on OH radicals' production as previously described by other authors. O_2 also traps excited electrons, thus decreasing recombination rates and generating oxygen centered radicals, such as superoxide ($O_2^{\bullet-}$) that also acts on the dye degradation.[42−44]

Reuse. Aiming at the practical application of the fibrous TiO_2-rich materials, the dye discoloration capability of the reused fibrous TiO_2 structures was evaluated for five catalytic cycles (Figure 4). The tests were run in the same conditions as the batch experiments under UVA/visible irradiation. The dye bleaching was measured after 3 h by measuring the absorbance at 440 nm and compared with the initial absorbance. All materials kept similar degradation capabilities, even after 5 cycles. TNF efficiency went from 61 to 65%, TGW dropped from 89 to 78% and TGF from 88 to 81%. The slight decrease in degradation efficiency for TGW and TGF may reflect some TiO_2 leaching from the supported materials, something that did not happen with TNF, which is made of 100% TiO_2.

Continuous Flow Degradation. Solutions for photocatalytic water treatment are ideally processed under a continuous flow using a fixed bed catalyst that allows for uniform light distribution, easy scale-up, fast mixing, and faster reactions. Here, we compared the performance of our three fibrous materials using crocin as our surrogate dye. Using a single-pass approach, we evaluated the performance of the catalysts at 4 different flow rates, 10, 30, 50, and 100 mL/h. The summary of the removal efficiency in the different flow rates can be seen in Figure 5. Overall, slower flow rates lead to

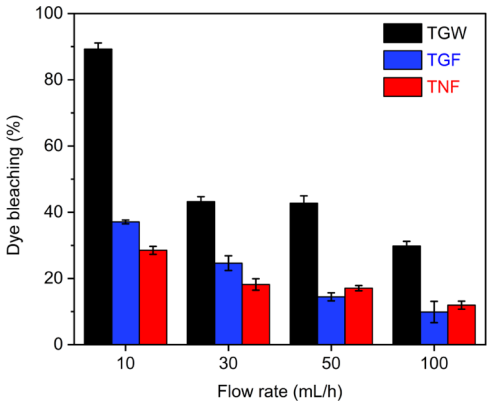

Figure 5. Crocin bleaching (%) using TGW (black), TGF (blue), or TNF (red) in a continuous flow system.

higher degradation, which is attributed to the longer residence/irradiation time (RT). A similar trend was also observed in previous reports for the degradation of other dyes like azo compounds and methyl orange.[45−47]

Since we chose to use the same TiO_2 amount for all catalysts, the volumes of each fibrous material were different inside the tubes, changing the residence time (RT) for the catalysts analyzed. All fibrous materials were able to be used in the flow system and were capable to bleach the dye in shorter times. In general, for all rates, TGW outperformed the other photocatalyst with maximum dye removal of 89% at 10 mL/h.

https://doi.org/10.1021/acsomega.3c00781
ACS Omega 2023, 8, 21585−21593

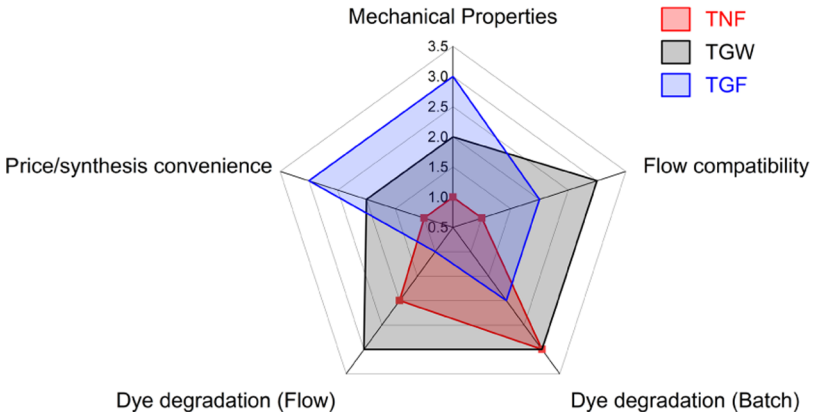

Figure 6. Radar plot of the fibrous catalysts for a relative comparison according to their physical features and chemical activity. The TiO_2-rich catalysts were ranked from 1 to 3 in the five categories, based on the results from this contribution.

As a comparison, at 50 mL/h, TGW bleached 43% of the dye with 35 s of RT, which would take at least 1 h of irradiation in our batch system. At the same flow rate, TGF removed 15% of the dye with an RT of 90 s and TNF removed 18% of the crocin with an RT of 115 s. The longer retention time together with better TiO_2 distribution resulted in better photocatalytic activity for TGW. TNF which also had high degradation rates in the batch experiments did not perform as well in flow. Continuous flow systems enable better light distribution favoring materials with higher volumes and better photocatalyst distribution such as TGW. On the other hand, TNF has a compact form due to the higher TiO_2 content not being as favorable with improvements in light distribution.

Interested on the results from the single-pass degradation, we selected the best working catalyst, TGW to observe the results from the degradations. After 90% bleaching at 440 nm, no color could be seen in the liquid. We then proceeded to observe the changes in the solution using HPLC. In Figure S15, we can see the HPLC peaks at 400 nm for the initial solution (in black). The conjugated structure of crocin allows for the formation of several isomers, which can be seen in peaks 1−5. Their absorbance profile (insert) shows similar absorbance spectra. After treatment with TGW and light, no other peak is visible proving the degradation of the molecule.

Catalyst Comparison. The development of suitable photocatalysts for water treatment reactors is a complex challenge that comprises catalytic performance, durability, cost efficiency, and range of action, among others.[48] In this study, we investigated and compared three fibrous TiO_2-rich structures that are suitable for flow systems. Aiming for their real-life application, we selected five categories, mechanical properties, price/synthesis convenience, dye degradation in batch and flow, as well as compatibility with flow systems and ranked the three catalysts from 1 to 3 for each of those categories. The data were then plotted in a radar plot for easy visualization.

The first category is mechanical properties, which we compared as how easy it is to manipulate those materials. For example, TNF are made of 100% TiO_2 which is a brittle material that can be easily broken when moved between surfaces and added into the treatment tubes. In contrast, TGF is a flexible paper that can be easily manipulated and breaks less easily. The second aspect evaluated is how flow-compatible are those materials. This category considers how easy it is to position them into glass flow tubes and how stable they are inside those tubes. In this category, TNF also scored lower than the other materials since it can be broken when transferred into the tubes and it tends to move with the flow. Both glass-supported TiO_2 materials were easier to insert into tubes and retain inside as the liquid flows. In particular, TGW, which ranks in the first place for this criterion, can be easily packed into the tubes, allowing the use of more catalysts, and can take different shapes adapting to the system being used. Moving to dye degradation performance in batch tests, we compared their performance bleaching crocin under UVA/visible (~400 nm) irradiation. Using the data displayed in Figure 3, we can see that TNF had a higher degradation rate under light irradiation, followed by TGW and TGF. Higher degradation rates mean that short treatment times are necessary using the same amount of catalyst.

Finally, we ranked the catalysts according to their synthesis convenience (availability, cost, scalability, and safety). TNF are synthesized using electrospinning that required high voltages together with flammable solvents. Although it is a low-cost technique,[49] it imposes a fire hazard that requires specialized labor and higher safety environments. For safety reasons, TNF was placed last in this category. Moving to TGW, the synthesis is done inside a glass tube, which does not require any special apparatus or equipment. However, glass wool must be treated with acid (HCl), followed by APTES attachment and overnight treatment with TiO_2 precursors. Compared to the other methods, it takes longer to obtain the final material. However, it is important to emphasize that the synthesis of TGW can be easily scaled up. Lastly, TGF came in first for this category as there is no prepreparation of the supporting material. The high surface area of the commercial glass fiber filter allows for effective TiO_2 deposition. Moreover, the material can be cut and shaped in the desired size, and TiO_2 precursors are added using a clothing iron, proving to be a simpler and inexpensive solution. Note that calcination treatment was not used as a comparison since all of the materials undergo similar processes.

Based on the radar plot (Figure 6), the catalysts were divided into two main categories, chemical descriptors, which are related to their catalytic activity, with TGW and TNF shown in the upper level of the right and bottom quadrants. On the other hand, there are physical descriptors, which are associated with the mechanical and synthetic aspects. In this case, TGF was placed in the upper level of the left and upper quadrants. The exception is TGW that took the upper level of

https://doi.org/10.1021/acsomega.3c00781
ACS Omega 2023, 8, 21585−21593

flow compatibility, which makes it a great candidate for flow applications due to its high performance and compatibility with continuous flow reactors.

CONCLUSIONS

The photochemical treatment of contaminated water requires the discovery of safe, durable, and cost-efficient catalysts that can operate in the UVA or visible regions. The materials reported here operate at the edge of these spectral regions, are fully compatible with flow methods, and can be prepared from readily available materials. Among the materials tested here, glass wool is the recommended support for flow-related applications, although glass filter materials offer some advantages relating to mechanical and synthetic properties, for example, no APTES treatment is required. The dye crocin serves as an excellent screening material, although ultimately the complete photodegradation of drug contaminants and the potential killing of bacteria will need to be evaluated. Overall, the three new photocatalysts studied offer a major advantage over the powder catalysts frequently used.

ASSOCIATED CONTENT

Supporting Information

The Supporting Information is available free of charge at https://pubs.acs.org/doi/10.1021/acsomega.3c00781.

Photographs of the materials studied, additional SEM images including EDS mapping, Tauc plots, and hydroxyl radical tests using a coumarin probe (PDF)

AUTHOR INFORMATION

Corresponding Authors

Tebello Nyokong − *Institute for Nanotechnology Innovation, Rhodes University, Grahamstown 6140, South Africa;* orcid.org/0000-0002-4590-9926; Email: t.nyokong@ru.ac.za

Juan C. Scaiano − *Department of Chemistry and Biomolecular Sciences, University of Ottawa, Ottawa, Ontario K1N 6N5, Canada;* orcid.org/0000-0002-4838-7123; Email: jscaiano@uottawa.ca

Authors

Daliane R. C. da Silva − *Department of Chemistry and Biomolecular Sciences, University of Ottawa, Ottawa, Ontario K1N 6N5, Canada*

Sivuyisiwe Mapukata − *Institute for Nanotechnology Innovation, Rhodes University, Grahamstown 6140, South Africa*

Sara Currie − *Department of Chemistry and Biomolecular Sciences, University of Ottawa, Ottawa, Ontario K1N 6N5, Canada*

Alexandros A. Kitos − *Department of Chemistry and Biomolecular Sciences, University of Ottawa, Ottawa, Ontario K1N 6N5, Canada*

Anabel E. Lanterna − *Department of Chemistry and Biomolecular Sciences, University of Ottawa, Ottawa, Ontario K1N 6N5, Canada;* Present Address: School of Chemistry, University of Nottingham, University Park, Nottingham NG7 2RD, U.K

Complete contact information is available at: https://pubs.acs.org/10.1021/acsomega.3c00781

Notes

The authors declare no competing financial interest.

ACKNOWLEDGMENTS

This work was supported by the Natural Sciences and Engineering Research Council of Canada, the Canada Foundation for Innovation, the Canada Research Chairs Program, the International Development Research Centre (IDRC, Canada), the Department of Science and Technology (DST) Innovation, and the National Research Foundation (NRF), South Africa through DST/NRF South African Research Chairs Initiative for Professor of Medicinal Chemistry and Nanotechnology (UID 62620). Thanks are due to Professor Muralee Murugesu for facilitating the BET studies and to Drs E. Alarcon, M. Muñoz, and S. Schejtman for help with the FTIR measurements.

REFERENCES

(1) WHO; UNICEF; Bank, W.. State of the World's Drinking Water: an Urgent Call to Action to Accelerate Progress on Ensuring Safe Drinking Water for All; 9789240060807; Geneva, 2022.

(2) Ding, Q.; Li, C.; Wang, H.; Xu, C.; Kuang, H. Electrochemical detection of heavy metal ions in water. *Chem. Commun* **2021**, *57*, 7215.

(3) Chakraborti, D.; Rahman, M. M.; Paul, K.; Chowdhury, U. K.; Sengupta, M. K.; Lodh, D.; Chanda, C. R.; Saha, K. C.; Mukherjee, S. C. Arsenic calamity in the Indian subcontinent: What lessons have been learned? *Talanta* **2002**, *58*, 3−22.

(4) Menon, N. G.; George, L.; Tatiparti, S. S. V.; Mukherji, S. Efficacy and reusability of mixed-phase TiO_2−ZnO nanocomposites for the removal of estrogenic effects of 17β-Estradiol and 17α-Ethinylestradiol from water. *J. Environ. Manage.* **2021**, *288*, 112340.

(5) Sun, J.; Luo, Q.; Wang, D.; Wang, Z. Occurrences of pharmaceuticals in drinking water sources of major river watersheds, China. *Ecotoxicol. Environ. Saf.* **2015**, *117*, 132−140.

(6) Ternes, T. A.; Meisenheimer, M.; McDowell, D.; Sacher, F.; Brauch, H. J.; Haist-Gulde, B.; Preuss, G.; Wilme, U.; Zulei-Seibert, N. Removal of pharmaceuticals during drinking water treatment. *Environ. Sci. Technol.* **2002**, *36*, 3855−3863.

(7) Kamat, P. V.; Sivula, K. Celebrating 50 Years of Photocatalytic Hydrogen Generation. *ACS Energy Lett.* **2022**, *7*, 3149−3150.

(8) Fujishima, A.; Honda, K. Electrochemical Photolysis of Water at a Semiconductor Electrode. *Nature* **1972**, *238*, 37−38.

(9) Ge, M.; Cao, C.; Huang, J.; Li, S.; Chen, Z.; Zhang, K.-Q.; Al-Deyab, S. S.; Lai, Y. A review of one-dimensional TiO_2 nanostructured materials for environmental and energy applications. *J. Mater. Chem. A* **2016**, *4*, 6772−6801.

(10) Tang, Z.-R.; Li, F.; Zhang, Y.; Fu, X.; Xu, Y.-J. Composites of Titanate Nanotube and Carbon Nanotube as Photocatalyst with High Mineralization Ratio for Gas-Phase Degradation of Volatile Aromatic Pollutant. *J. Phys. Chem. C* **2011**, *115*, 7880−7886.

(11) Jothi Prakash, C. G.; Prasanth, R. 7 - TiO2-based devices for energy-related applications. In *Titanium Dioxide (TiO_2) and Its Applications*; Parrino, F.; Palmisano, L., Eds.; Elsevier, 2021; pp 241−265.

(12) Dell'Edera, M.; Lo Porto, C.; De Pasquale, I.; Petronella, F.; Curri, M. L.; Agostiano, A.; Comparelli, R. Photocatalytic TiO2-based coatings for environmental applications. *Catal. Today* **2021**, *380*, 62−83.

(13) Mohadesi, M.; Sanavi Fard, M.; Shokri, A. The application of modified nano-TiO_2 photocatalyst for wastewater treatment: A review. *Int. J. Environ. Anal. Chem.* **2022**, 1−22.

(14) Horikoshi, S.; Serpone, N. Can the photocatalyst TiO_2 be incorporated into a wastewater treatment method? Background and prospects. *Catal. Today* **2020**, *340*, 334−346.

(15) Riaz, S.; Park, S.-J. An overview of TiO_2-based photocatalytic membrane reactors for water and wastewater treatments. *J. Ind. Eng. Chem.* **2020**, *84*, 23−41.
(16) Yaghmaei, M.; Lanterna, A. E.; Scaiano, J. C. Nitro to amine reductions using aqueous flow catalysis under ambient conditions. *iScience* **2021**, *24*, 103472.
(17) Tatsuma, T.; Tachibana, S. I.; Miwa, T.; Tryk, D. A.; Fujishima, A. Remote Bleaching of Methylene Blue by UV-Irradiated TiO2 in the Gas Phase. *J. Phys. Chem. B* **1999**, *103*, 8033−8035.
(18) Sun, Q.; Li, K.; Wu, S.; Han, B.; Sui, L.; Dong, L. Remarkable improvement of TiO_2 for dye photocatalytic degradation by a facile post-treatment. *New J. Chem.* **2020**, *44*, 1942−1952.
(19) Lee, S. Y.; Kang, D.; Jeong, S.; Do, H. T.; Kim, J. H. Photocatalytic Degradation of Rhodamine B Dye by TiO_2 and Gold Nanoparticles Supported on a Floating Porous Polydimethylsiloxane Sponge under Ultraviolet and Visible Light Irradiation. *ACS Omega* **2020**, *5*, 4233−4241.
(20) Naskar, S.; Pillay, S. A.; Chanda, M. Photocatalytic Degradation of Organic Dyes in Aqueous Solution with TiO_2 Nanoparticles Immobilized on Foamed Polyethylene Sheet. *J. Photochem. Photobiol., A* **1998**, *113*, 257−264.
(21) Oliveira, G. H.; Galante, M. T.; Martins, T. T.; dos Santos, L. F. L. S.; Ely, F.; Longo, C.; Gonçalves, R. V.; Muniz, S. R.; Nome, R. A. Real time single TiO_2 nanoparticle monitoring of the photodegradation of methylene blue. *Solar Energy* **2019**, *190*, 239−245.
(22) Barton, I.; Matejec, V.; Matousek, J. Photocatalytic activity of nanostructured TiO_2 coating on glass slides and optical fibers for methylene blue or methyl orange decomposition under different light excitation. *J. Photochem. Photobiol., A* **2016**, *317*, 72−80.
(23) Elhage, A.; Wang, B.; Marina, N.; Marin, M. L.; Cruz, M.; Lanterna, A. E.; Scaiano, J. C. Glass wool: a novel support for heterogeneous catalysis. *Chem. Sci.* **2018**, *9*, 6844−6852.
(24) Lu, Y.; Ou, X.; Wang, W.; Fan, J.; Lv, K. Fabrication of TiO_2 nanofiber assembly from nanosheets (TiO2-NFs-NSs) by electrospinning-hydrothermal method for improved photoreactivity. *Chin. J. Catal.* **2020**, *41*, 209−218.
(25) Mapukata, S.; Hainer, A. S.; Lanterna, A. E.; Scaiano, J. C.; Nyokong, T. Decorated titania fibers as photocatalysts for hydrogen generation and organic matter degradation. *J. Photochem. Photobiol., A* **2020**, *388*, No. 112185.
(26) Lou, L.; Kendall, R. J.; Ramkumar, S. Comparison of hydrophilic PVA/TiO_2 and hydrophobic PVDF/TiO2 microfiber webs on the dye pollutant photo-catalyzation. *J. Environ. Chem. Eng.* **2020**, *8*, No. 103914.
(27) Shen, C.; Wang, Y. J.; Xu, J. H.; Luo, G. S. Facile synthesis and photocatalytic properties of TiO_2 nanoparticles supported on porous glass beads. *Chem. Eng. J* **2012**, *209*, 478−485.
(28) Uddin, M. J.; Cesano, F.; Bonino, F.; Bordiga, S.; Spoto, G.; Scarano, D.; Zecchina, A. Photoactive TiO_2 films on cellulose fibres: synthesis and characterization. *J. Photochem. Photobiol., A* **2007**, *189*, 286−294.
(29) Lan, L.; Daly, H.; Jiao, Y.; Yan, Y.; Hardacre, C.; Fan, X. Comparative study of the effect of TiO_2 support composition and Pt loading on the performance of Pt/TiO_2 photocatalysts for catalytic photoreforming of cellulose. *Int. J. Hydrogen Energy* **2021**, *46*, 31054−31066.
(30) Meroni, D.; Lo Presti, L.; Di Liberto, G.; Ceotto, M.; Acres, R. G.; Prince, K. C.; Bellani, R.; Soliveri, G.; Ardizzone, S. A Close Look at the Structure of the TiO_2-APTES Interface in Hybrid Nanomaterials and Its Degradation Pathway: An Experimental and Theoretical Study. *J. Phys. Chem. C* **2017**, *121*, 430−440.
(31) Chen, X.; Hosseini, S. N.; van Huis, M. A. Heating-Induced Transformation of Anatase TiO_2 Nanorods into Rock-Salt TiO Nanoparticles: Implications for Photocatalytic and Gas-Sensing Applications. *ACS Appl. Nano Mater.* **2022**, *5*, 1600−1606.
(32) Baiju, K. V.; Shukla, S.; Sandhya, K. S.; James, J.; Warrier, K. G. K. Photocatalytic Activity of Sol-Gel-Derived Nanocrystalline Titania. *J. Phys. Chem. C* **2007**, *111*, 7612−7622.
(33) Riegel, G.; Bolton, J. R. Photocatalytic efficiency variability in TiO_2 particles. *J. Phys. Chem. A* **1995**, *99*, 4215−4224.
(34) Kavan, L.; Grätzel, M.; Gilbert, S. E.; Klemenz, C.; Scheel, H. J. Electrochemical and Photoelectrochemical Investigation of Single-Crystal Anatase. *J. Am. Chem. Soc.* **1996**, *118*, 6716−6723.
(35) Thommes, M.; Kaneko, K.; Neimark, A. V.; Olivier, J. P.; Rodriguez-Reinoso, F.; Rouquerol, J.; Sing, K. S. W. Physisorption of gases, with special reference to the evaluation of surface area and pore size distribution (IUPAC Technical Report). *Pure Appl. Chem.* **2015**, *87*, 1051−1069.
(36) Kočí, K.; Obalová, L.; Matějová, L.; Plachá, D.; Lacný, Z.; Jirkovský, J.; Šolcová, O. Effect of TiO2 particle size on the photocatalytic reduction of CO_2. *Appl. Catal., B* **2009**, *89*, 494−502.
(37) Vickackaite, V.; Romani, A.; Pannacci, D.; Favaro, G. Photochemical and thermal degradation of a naturally occurring dye used in artistic painting. A chromatographic, spectrophotometric and fluorimetric study on saffron, 2004.
(38) Winterhalter, P.; Straubinger, M. Saffron—renewed interest in an ancient spice. *Food Rev. Int.* **2000**, *16*, 39−59.
(39) Ma, Y.; Yao, J.-n. Photodegradation of Rhodamine B catalyzed by TiO_2 thin films. *J. Photochem. Photobiol., A* **1998**, *116*, 167−170.
(40) Ishibashi, K.-i.; Fujishima, A.; Watanabe, T.; Hashimoto, K. Quantum yields of active oxidative species formed on TiO_2 photocatalyst. *J. Photochem. Photoniol., A: Chem.* **2000**, *134*, 139−142.
(41) Leandri, V.; Gardner, J. M.; Jonsson, M. Coumarin as a Quantitative Probe for Hydroxyl Radical Formation in Heterogeneous Photocatalysis. *J. Phys. Chem. C* **2019**, *123*, 6667−6674.
(42) Hayyan, M.; Hashim, M. A.; AlNashef, I. M. Superoxide Ion: Generation and Chemical Implications. *Chem. Rev.* **2016**, *116*, 3029−3085.
(43) Holroyd, R. A.; Bielski, B. H. J. Photochemical generation of superoxide radicals in aqueous solutions. *J. Am. Chem. Soc.* **1978**, *100*, 5796−5800.
(44) Galindo, C.; Jacques, P.; Kalt, A. Photodegradation of the aminoazobenzene acid orange 52 by three advanced oxidation processes: UV/H2O2, UV/TiO2 and VIS/TiO_2: Comparative mechanistic and kinetic investigations. *J. Photochem. Photobiol., A* **2000**, *130*, 35−47.
(45) Mahmoodi, N. M.; Arami, M.; Limaee, N. Y.; Tabrizi, N. S. Decolorization and aromatic ring degradation kinetics of Direct Red 80 by UV oxidation in the presence of hydrogen peroxide utilizing TiO_2 as a photocatalyst. *Chem. Eng. J.* **2005**, *112*, 191−196.
(46) Behnajady, M. A.; Modirshahla, N.; Daneshvar, N.; Rabbani, M. Photocatalytic degradation of an azo dye in a tubular continuous-flow photoreactor with immobilized TiO_2 on glass plates. *Chem. Eng. J.* **2007**, *127*, 167−176.
(47) Zhang, X.; Su, X.; Gao, W.; Wang, F.; Liu, Z.; Zhan, J.; Liu, B.; Wang, R.; Liu, H.; Sang, Y.; Zhang, X. Photocatalytic quartz fiber felts with carbon-connected TiO_2 nanoparticles for capillarity-driven continuous-flow water treatment Graphical abstract. *Appl. Phys. A* **2018**, *124*, No. 459.
(48) Chong, M. N.; Jin, B.; Chow, C. W. K.; Saint, C. Recent developments in photocatalytic water treatment technology: A review. *Water Res.* **2010**, *44*, 2997−3027.
(49) Cui, J.; Li, F.; Wang, Y.; Zhang, Q.; Ma, W.; Huang, C. Electrospun nanofiber membranes for wastewater treatment applications. *Sep. Purif. Technol.* **2020**, *250*, No. 117116.

https://doi.org/10.1021/acsomega.3c00781
ACS Omega 2023, 8, 21585−21593